Supplementary Information for the manuscript titled "Electrophoretic trajectories of non-uniformly charged particles in viscoelastic fluids: The weak surface charge limit"

Rajnandan Borthakur[1] and Uddipta Ghosh[1]

[1]*Discipline of Mechanical Engineering, Indian Institute of Technology Gandhinagar, Palaj - 382355, Gujarat, India*

This supplementary material is structured as follows. In §S1, we provide the detailed expressions of the convected derivatives to complement §3 in the main article. In §S2, we have shown the temporal evolution of the surface change with time using contour plots, when higher order harmonics are included in the surface charge. This is complementary to §5.2 in the manuscript. Finally, in §S3, we have outlined the temporal variations in the integrals $\mathcal{J}_{HS}$ and $\mathcal{J}_{Bulk}$ appearing in the expression of $\boldsymbol{\Omega}_2$ and defined in eqn. (5.3b) in the main article. This section complements figure 7 in the main manuscript.

S1 The Convected derivatives

In this section, we shall provide the expressions of the various components of the convected derivative $\boldsymbol{\mathcal{S}}_2$ of the leading order strain rate tensor $\boldsymbol{D}_1$, which are necessary for calculating the $O(\overline{\zeta}_0^2)$ particle velocities [1].

$$\mathcal{S}_{rr,2} = (\boldsymbol{v}_1.\nabla)D_{rr,1} - 2\left\{\frac{\partial v_{r,1}}{\partial r}D_{rr,1} - \frac{1}{r}\sqrt{1-\eta^2}\frac{\partial v_{r,1}}{\partial \eta}D_{r\theta,1} + \frac{1}{r\sqrt{1-\eta^2}}\frac{\partial v_{r,1}}{\partial \phi}D_{r\phi,1}\right\} \tag{S1}$$

$$\begin{aligned}\mathcal{S}_{\theta\theta,2} &= (\boldsymbol{v}_1.\nabla)D_{\theta\theta,1} + 2\left\{D_{r\theta,1}\left(\frac{v_{\theta,1}}{r} - \frac{\partial v_{\theta,1}}{\partial r}\right) + D_{\theta\theta,1}\left(\frac{1}{r}\sqrt{1-\eta^2}\frac{\partial v_{\theta,1}}{\partial \eta} - \frac{v_{r,1}}{r}\right)\right. \\ &\quad \left. -D_{\phi\theta,1}\frac{1}{r\sqrt{1-\eta^2}}\frac{\partial v_{\theta,1}}{\partial \phi}\right\}\end{aligned} \tag{S2}$$

$$\begin{aligned}\mathcal{S}_{\phi\phi,2} &= (\boldsymbol{v}_1.\nabla)D_{\phi\phi,1} + 2\left\{D_{r\phi,1}\left(\frac{v_{\phi,1}}{r} - \frac{\partial v_{\phi,1}}{\partial r}\right) + D_{\theta\phi,1}\left(\frac{v_{\phi,1}\eta}{r\sqrt{1-\eta^2}} + \frac{1}{r}\sqrt{1-\eta^2}\frac{\partial v_{\phi,1}}{\partial \eta}\right)\right. \\ &\quad \left. -D_{\phi\phi,1}\left(\frac{1}{r\sqrt{1-\eta^2}}\frac{\partial v_{\phi,1}}{\partial \phi} + \frac{v_{r,1}}{r} + \frac{v_{\theta,1}\eta}{r\sqrt{1-\eta^2}}\right)\right\}\end{aligned} \tag{S3}$$

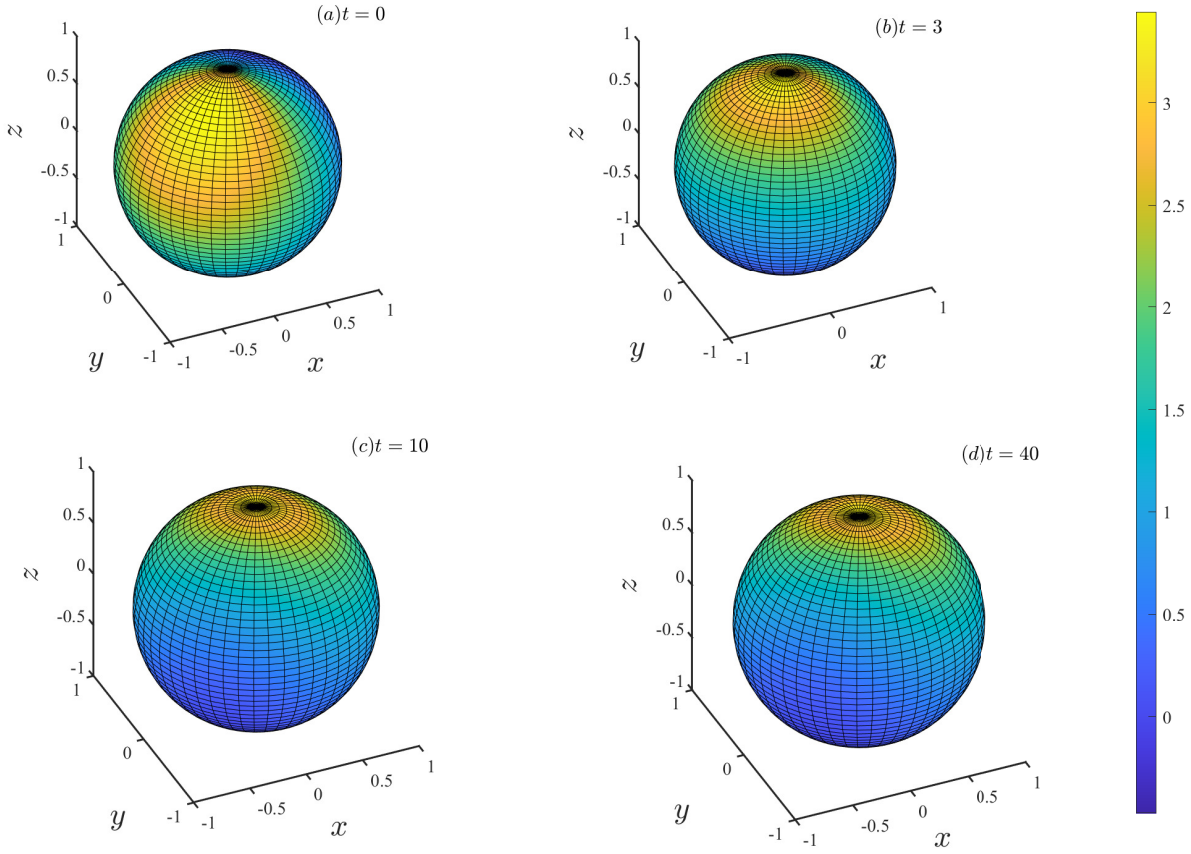

Figure S1: Contour plot of the surface charge $\breve{\zeta}(\theta, \phi, t)$ distribution, initially same as that in fig. 5 in the main article, at four different times: (a) $t = 0$ (initial distribution); (b) $t = 3$ (intermediate); (c) $t = 10$ (rotation slowed down) and (d) $t = 40$ (steady state), to underline its dynamically evolving nature. We have chosen $De = 1$. Other relevant parameters are also identical to those in fig. 5 in the manuscript.

$$\begin{aligned}\mathcal{S}_{r\theta,2} &= (\boldsymbol{v}_1.\nabla)D_{r\theta,1} + D_{rr,1}\left(\frac{v_{\theta,1}}{r} - \frac{\partial v_{\theta,1}}{\partial r}\right) + D_{r\theta,1}\left(\frac{1}{r}\sqrt{1-\eta^2}\frac{\partial v_{\theta,1}}{\partial \eta} - \frac{\partial v_{r,1}}{\partial r} - \frac{v_{r,1}}{r}\right) \\ &\quad + D_{\theta\theta,1}\left(\frac{1}{r}\sqrt{1-\eta^2}\frac{\partial v_{r,1}}{\partial \eta}\right) - \frac{1}{r\sqrt{1-\eta^2}}\frac{\partial v_{r,1}}{\partial \phi}D_{\phi\theta,1} - \frac{1}{r\sqrt{1-\eta^2}}\frac{\partial v_{\theta,1}}{\partial \phi}D_{r\phi,1} \qquad \text{(S4)}\end{aligned}$$

$$\begin{aligned}\mathcal{S}_{r\phi,2} &= (\boldsymbol{v}_1.\nabla)D_{r\phi,1} + D_{rr,1}\left(\frac{v_{\phi,1}}{r} - \frac{\partial v_{\phi,1}}{\partial r}\right) + D_{r\theta,1}\left(\frac{v_{\phi,1}\eta}{r\sqrt{1-\eta^2}} + \frac{1}{r}\sqrt{1-\eta^2}\frac{\partial v_{\phi,1}}{\partial \eta}\right) - \\ &\quad D_{r\phi,1}\left(\frac{\partial v_{r,1}}{\partial r} + \frac{1}{r\sqrt{1-\eta^2}}\frac{\partial v_{\phi,1}}{\partial \phi} + \frac{v_{r,1}}{r} + \frac{v_{\theta,1}\eta}{r\sqrt{1-\eta^2}}\right) + D_{\theta\phi,1}\frac{1}{r}\sqrt{1-\eta^2}\frac{\partial v_{r,1}}{\partial \eta} \\ &\quad - D_{\phi\phi,1}\frac{1}{r\sqrt{1-\eta^2}}\frac{\partial v_{r,1}}{\partial \phi} \qquad \text{(S5)}\end{aligned}$$

$$\begin{aligned}\mathcal{S}_{\theta\phi,2} &= (\boldsymbol{v}_1.\nabla)D_{\theta\phi,1} + D_{r\theta,1}\left(\frac{v_{\phi,1}}{r} - \frac{\partial v_{\phi,1}}{\partial r}\right) + D_{\theta\theta,1}\left(\frac{v_{\phi,1}\eta}{r\sqrt{1-\eta^2}} + \frac{1}{r}\sqrt{1-\eta^2}\frac{\partial v_{\phi,1}}{\partial \eta}\right) + \\ &\quad D_{\theta\phi,1}\left(\frac{1}{r}\sqrt{1-\eta^2}\frac{\partial v_{\theta,1}}{\partial \eta} - \frac{2v_{r,1}}{r} - \frac{1}{r}\sqrt{1-\eta^2}\frac{\partial v_{\phi,1}}{\partial \phi} - \frac{v_{\theta,1}\eta}{r\sqrt{1-\eta^2}}\right)\end{aligned}$$

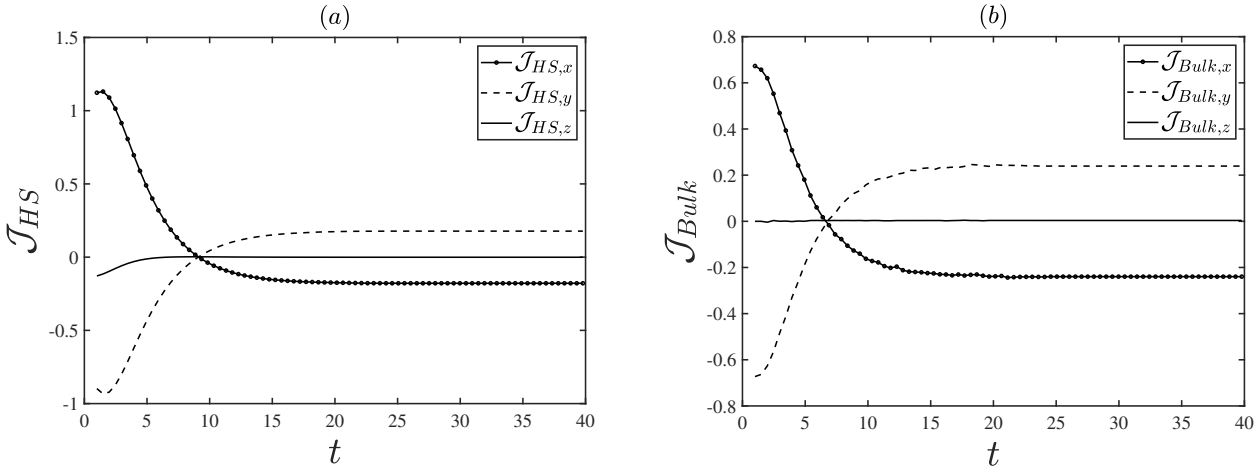

Figure S2: Evolution of the integrals $\mathcal{J}_{HS}$ (in (a)) and $\mathcal{J}_{Bulk}$ (in (b)), defined in eqn. (5.3a) in the main article, along x, y and z have been plotted with time. We have chosen $De = 1$. The initial distribution of $\breve{\zeta}(\theta, \phi)$ and all other relevant parameters are the same as in figure 7.

$$+D_{r\phi,1}\left(\frac{v_{\theta,1}}{r} - \frac{\partial v_{\theta,1}}{\partial r}\right) - D_{\phi\phi,1}\frac{1}{r\sqrt{1-\eta^2}}\frac{\partial v_{\theta,1}}{\partial \phi} \tag{S6}$$

where

$$(\boldsymbol{v}_1.\nabla) = v_{r,1}\frac{\partial}{\partial r} - \frac{v_{\theta,1}}{r}\sqrt{1-\eta^2}\frac{\partial}{\partial \eta} + \frac{v_{\phi,1}}{r\sqrt{1-\eta^2}}\frac{\partial}{\partial \phi}$$

S2 Temporal evolution of the surface charge

Figure S1, illustrates the temporal evolution of $\breve{\zeta}(\theta, \phi, t)$ by representing it as a contour plot at four different time instances: $t = 0$ (starting point) in (a), $t = 3$ in (b), $t = 10$ in (c) and $t = 40$ in (d) - all other parameters as well as the starting distribution of $\breve{\zeta}(\theta, \phi, t = 0)$ remain identical to those in figure 5 of the main article. It is observed that overall, the surface charge evolves in much the same way as shown in figure 4 of the manuscript. Initially, the dipole moment is not directed along the imposed electric field and hence the particle rotates until $\boldsymbol{H}_1^{(1)}$ and $\boldsymbol{E}_\infty$ become co-linear, after which the rotation stops. This occurs after approximately $t \approx 15$ and thus it may be observed from panels (c) and (d) that $\breve{\zeta}(\theta, \phi, t)$ barely changes between times $t = 10$ and 40. However, in the present scenario, the particle does not contain any natural axis of symmetry and hence unline in figure 4 of the main article, here the steady state distribution of $\breve{\zeta}$ is not axisymmetric, as evident from panel (d).

S3 Plots of the integrals appearing in $\boldsymbol{\Omega}_2$ in eqn. (5.3b) in the main article

Figure S2 demonstrates the variations in $\mathcal{J}_{HS}$ (panel (a)) and $\mathcal{J}_{Bulk}$ (panel (b)) along the three directions, appearing in the expression for $\boldsymbol{\Omega}_2$ and defined in eqn. (5.3b) in the main article. The choice of initial $\breve{\zeta}(\theta, \phi, t)$ as well as other parameters remains identical to those in figure 7 in the manuscript. We reiterate that $\mathcal{J}_{HS}$ underlines the effect of excess polymeric stresses from within the EDL, while $\mathcal{J}_{Bulk}$ indicates those from the bulk. It is observed that during the initial phases, contributions from $\mathcal{J}_{HS}$, i.e., the stresses within the EDL is larger than $\mathcal{J}_{Bulk}$

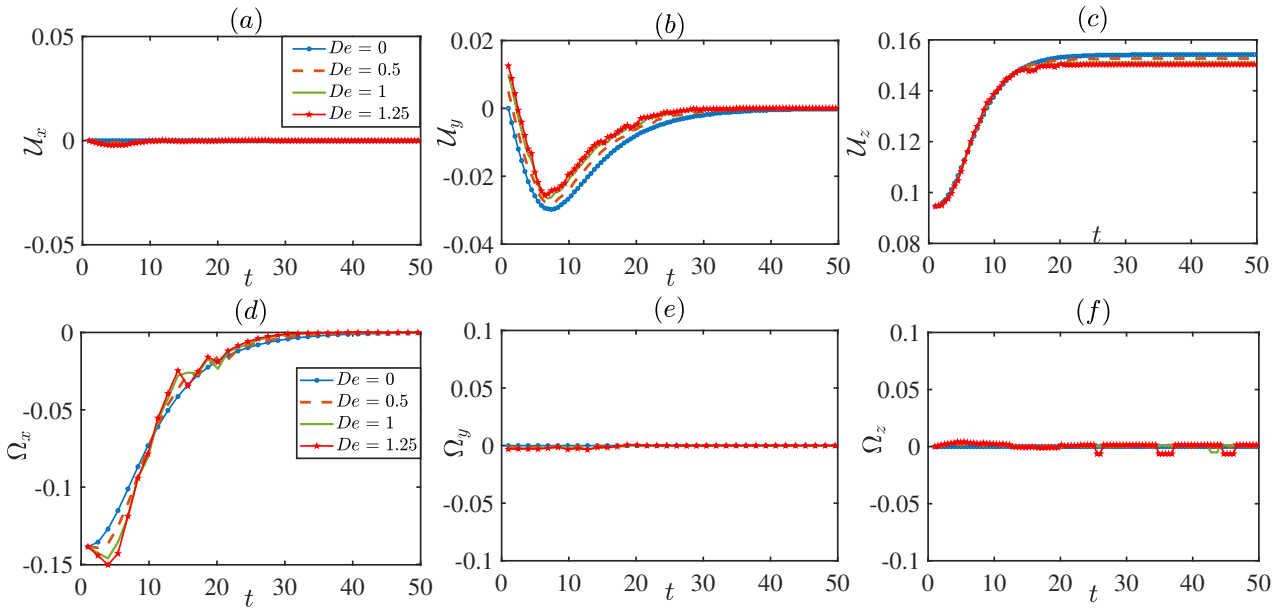

Figure S3: Plot of the translational velocity components ((a) $\mathcal{U}_x$, (b) $\mathcal{U}_y$ and (c) $\mathcal{U}_z$) and the angular velocity components ((d) Ω_x, (e) Ω_y and (f) Ω_z) of the particle as a function of time for various choices of $De = 0,\ 0.5,\ 1$ and1.25. The initial surface charge distribution ($\breve{\zeta}(\theta, \phi, t = 0)$) as well as the other parameters remain identical to those in fig. 9 in the main article.

and this forces the particle to rotate. As time progresses however, the excess polymeric stresses in the bulk ($\mathcal{J}_{Bulk}$) eventually catch up and hence the two exactly cancel each other out so that the particle stops rotating. At this point, the dipole moment of the surface charge also becomes co-linear with the imposed electric field.

S4 Temporal variations in $\mathcal{U}$ and Ω for the Janus particle

Figure S3 demonstrates the temporal variations in the translational and angular velocity components for the Janus particle considered in §5.3 and figure 9 in the main article. The panel-wise description remains identical to those in figure 3 of the main article. Although the overall trends shown by both translational and angular velocities remain same as in figures 3 and 6 of the main article, it is interesting to note that here, all the translational velocity components ($\mathcal{U}_x$, $\mathcal{U}_y$ and $\mathcal{U}_z$) decrease with De (in contrast to what is observed in figures 3 and 6 in the main article), which results from the viscoelastic and the Newtonian contributions to the migration velocities (especially $\mathcal{U}_y$) opposing each other. This finally leads to a suppression of the migration along the y-direction in a viscoelastic medium, as also noted in the main article.

References

[1] Robert Byron Bird, Robert Calvin Armstrong, and Ole Hassager. Dynamics of polymeric liquids. vol. 1: Fluid mechanics. 1987.